Carbohydrate Polymers 83 (2011) 186–191

Contents lists available at ScienceDirect

Carbohydrate Polymers

journal homepage: www.elsevier.com/locate/carbpol

Preparation and properties of halloysite nanotubes/plasticized *Dioscorea opposita* Thunb. starch composites

Yanfang Xie [a], Peter R. Chang [b], Shujun Wang [c], Jiugao Yu [a], Xiaofei Ma [a,*]

[a] *Chemistry Department, School of Science, Tianjin University, Tianjin 300072, China*
[b] *Bioproducts and Bioprocesses National Science Program, Agriculture and Agri-Food Canada, 107 Science Place, Saskatoon, SK, S7N 0X2, Canada*
[c] *School of Pharmaceutical Science and Technology, Tianjin University, Tianjin 300072, China*

ARTICLE INFO

Article history:
Received 7 July 2010
Received in revised form 19 July 2010
Accepted 19 July 2010
Available online 27 July 2010

Keywords:
Halloysite nanotube
Starch
Dioscorea opposita Thunb.

ABSTRACT

A traditional Chinese medicine, *Dioscorea opposita* Thunb. is rich in starch, which was isolated and used to prepare the plasticized starch (PS). And PS was composited with halloysite nanotube (HNT) by the casting process. Amylose content of native starch was about 24.5%, and the granules were in the size of about 20 μm. The starch showed the typical B-type with relative crystallinity of 26.9%. According to the characterization of the composites with scanning electron microscope, mechanical tensile testing, rapid visco-analyser, thermogravimetric analysis and water vapor permeability, HNT could obviously improve the pasting viscosity, mechanical properties, thermal stability and water vapor barrier of the composites. When HNT contents varied from 0 to 9 wt%, the tensile strength increased from 3.9 to 9.7 MPa, and the water vapor permeability decreased from 8.48×10^{-10} to 6.61×10^{-10} g m^{-1} s^{-1} Pa^{-1} at RH 75% and from 14.54×10^{-10} to 11.7×10^{-10} g m^{-1} s^{-1} Pa^{-1} at RH 100%.

1. Introduction

Halloysite is a natural aluminosilicate nanotube from a clay mineral with a similar structure to kaolinite. It has a two-layered aluminosilicate structure, in which the hollow tubular morphology is formed by layer rolling. Halloysite nanotube (HNT) exhibits a high aspect ratio with the length of 1–15 μm and an inner diameter of 10–150 nm (Shchukin, Sukhorukov, Price, & Lvov, 2005). Compared to carbon nanotube (CNT), HNTs are easily available and much cheaper. HNTs also have a wide variety of biological and non-biological applications such as the storage of molecular hydrogen, catalytic conversions and processing of hydrocarbons, the absorbance on environmental hazardous species and urolithiasis treatment (Shamsi & Geckeler, 2008). It is different from CNT that the rod-like geometry of HNT never intertwines each other, which makes HNT disperse better in a polymer matrix. As a new nano-filler, HNT can obviously increase mechanical properties of epoxy/cyanate ester resin (Liu, Guo, Du, Cai, & Jia, 2007) and polypropylene (Liu, Guo, Du, Zou, & Du, 2008) matrix.

Dioscoreae, the rhizome of genus *D. opposita* Thunb., is one of traditional Chinese medicines (TCMs), named as Shanyao in Chinese. It has used to invigorate the spleen, stomach and kidney, promote production of the body fluids and benefit the lung (Wang et al., 2006). Starch is the main component in *D. opposita* Thunb., which contains about 43.7 wt% starch on average. Wang, Yu, Liu, & Chen (2008) have investigated the morphology, amylose content, swelling power, water-binding capacity, thermal and crystal properties of starches separated from different *D. opposita* Thunb. However, plasticized starch materials from *D. opposita* Thunb. have not been reported before. In order to extend the application of starch from *D. opposita* Thunb., HNT was firstly incorporated to plasticized starch (PS) to prepare the HNT/PS composites. This work was focused on the processing and characterization of HNT/PS composites in terms of morphology, mechanical properties, thermal stability and water vapor permeability.

2. Materials and methods

2.1. Materials

D. opposita Thunb. was purchased from Henan province, China. The HNTs were obtained from Hunan province, China. Glycerol, ethanol and sodium hydroxide were purchased from Tianjin Chemical Reagent Factory, China.

2.2. Isolation of starch

D. opposita Thunb. starch was isolated according to the modified method of Wang, Yu, Liu et al. (2008). The *D. opposita* Thunb. was dried, washed, cut into small pieces and milled to pass through

* Corresponding author. Tel.: +86 22 27406144; fax: +86 22 27403475.
E-mail address: maxiaofei@tju.edu.cn (X. Ma).

0144-8617/$ – see front matter © 2010 Elsevier Ltd. All rights reserved.
doi:10.1016/j.carbpol.2010.07.039

a 120 mesh sieve. The powders were immersed in aqueous solution containing 0.02% NaOH for 12 h. When starch was precipitated, the supernatant was removed. The starch was washed three times in distilled water. The slurry containing starch was centrifuged at 3000 rpm for 5 min. The supernatant and upper non-white layer, which contained the skin and cell wall, were removed. The white layer (starch layer) was washed three times. Finally, the starch was washed with ethanol. The starch samples were collected and dried overnight at 30 °C.

2.3. Processing of PS and PS/HNT composites

HNT were dispersed in a solution of distilled water (100 ml) and glycerol (1.5 g) and ultrasonicated for 0.5 h before adding 5 g starch. The load level of HNT filler (0, 1.5, 3, 6, 9 or 12 wt%) was based on 5 g starch. In order to plasticize starch, the mixture was heated at 90 °C for 0.5 h with constant stirring. The paste obtained was cast in a dish and dried at 50 °C for about 6 h with enhanced air circulation.

The composites were preconditioned in a climate chamber at 25 °C and RH 50% for at least 48 h prior to testing. Water content of the composites was about 10 wt%.

2.4. Amylose content

Amylose content of the isolated starch was determined in triplicate by using the method of Williams, Kuzina, and Hiynka, 1970 and Wang et al. (2007). The amylose from *D. opposita* Thunb. was separated by alkali leaching, purified, and used as a standard.

2.5. Differential scanning calorimetry (DSC)

The temperature range of gelatinization was measured using a differential scanning calorimeter DSC204, HP (NETZSCH, Germany) equipped with a thermal analysis station. Starch (about 10 mg) was weighed in the aluminium pan, and distilled water was added with a microliter syringe to obtain a starch-water suspension containing 70% water. The pan was hermetically sealed and held for 1 h at room temperature. The DSC analyzer was calibrated using indium and an empty aluminium pan was used as reference. Sample pans were heated at a rate of 10 °C/min from 20 to 120 °C. Onset temperature (T_o), peak temperature (T_p), conclusion temperature (T_c) and enthalpy of gelatinization (ΔH_{gel}) were calculated.

2.6. FTIR

FTIR spectra of starch and PS were performed at 2 cm^{-1} resolution with BIO-RAD FTS3000 IR Spectrum Scanner. Typically, 64 scans were signal-averaged to reduce spectral noise.

2.7. Scanning electron microscopy (SEM)

Starch powders and the fracture surfaces of PS were examined using a Scanning Electron Microscope Philips XL-3. The fracture surfaces of HNT/PS composites were tested by a Nanosem 430 Scanning Electron Microscope. Starch and HNT were respectively dispersed into ethanol using ultrasonication for 5 min. The suspension drops were drawn on a glass flake, dried to remove ethanol, and then vacuum coated with gold for SEM. PS and HNT/PS composites were cooled in liquid nitrogen, and then broken. The fracture faces were vacuum coated with gold for SEM.

2.8. X-ray diffraction

Starch powders were placed in a sample holder for XRD. XRD patterns were recorded in the reflection mode in angular range 4–30° (2θ) at the ambient temperature by a Panalytical X'Pert Pro diffractometer (PANalytical, Holland), operated at 45 kV and 30 mA with the Co-Kα radiation, $k = 0.178901$ nm. The degree of crystallinity of samples was quantitatively estimated, following the method of Wang, Yu, & Yu (2008).

2.9. Characteristics of starch pastes

The pasting properties were analyzed using a Rapid Visco Analyser (Newport Scientific, Sydney, Australia) according to AACC method 76-21 (Chang, Jian, Yu, & Ma, 2010). 1.5 g starch was dispersed into a solution of distilled water (25 ml). The obtained starch slurry was held at 50 °C for 1 min, then heated to 95 °C at 12.2 °C/min and held at 95 °C for 2.5 min. It was then cooled to 50 °C (cooling rate of 11.8 °C/min) and held at 50 °C for 2 min. The paddle speed was 960 rpm for 10 s and then decreased to 160 rpm for the remainder of the experiment.

2.10. Mechanical testing

The Testometric AX M350-10KN Materials Testing Machine was operated with a crosshead speed of 50 mm/min for tensile testing (ISO 1184-1983 standard). The result was the average of 5–8 specimens.

2.11. Thermogravimetric analysis

Thermal properties of the composites were measured with a ZTY-ZP type thermal analyzer. The films were broken with the weight of about 10 mg, and heated from room temperature to 500 °C at a heating rate of 15 °C/min in a nitrogen atmosphere.

2.12. Water vapor permeability (WVP)

WVP tests were carried out using ASTM method E96 (1996) with some modifications (Yu, Wang, & Ma, 2008). RH 0% was maintained using anhydrous calcium chloride in the cell. The samples were cut into circles and the cell sealed over with melted paraffin. Each cell was stored in a desiccator containing saturated sodium chloride solution or pure water to provide a constant RH 75% or 100% at 25 °C. WVP was determined by calculating the weight gain of the permeation cell. Changes in the weight of the cell were recorded as a function of time. Slopes were calculated by linear regression (weight change vs. time) and correlation coefficients for all reported data were >0.99. The water vapor transmission rate (WVTR) was defined as the slope (g/s) divided by the transfer area (m^2). After the permeation tests, film thickness was measured and WVP (g Pa^{-1} s^{-1} m^{-1}) was calculated as:

$$\mathrm{WVP} = \frac{\mathrm{WVTR}}{P(\mathrm{R}_1 - \mathrm{R}_2)} \times x$$

where P is the saturation vapor pressure of water (Pa) at the test temperature (25 °C), R_1 is the RH in the desiccator, R_2 is the RH in the permeation cell, and x is the film thickness (m). Under these conditions of RH 75% or 100%, the driving forces $P(R_1 - R_2)$ are respectively 1753.5 and 2338 Pa.

3. Results and discussion

3.1. Properties of D. opposita Thunb. starch

The properties of *D. opposita* Thunb. starch are listed as following: amylose content of *D. opposita* Thunb. starch is 24.5%, and the relative crystallinity is 26.9%. The transition temperatures (T_o, T_p, and T_c) are respectively 61.3, 65.5 and 69.6 °C, and the enthalpies of gelatinization (ΔH_{gel}) is 12.95 J/g. Here T_o, T_p, and

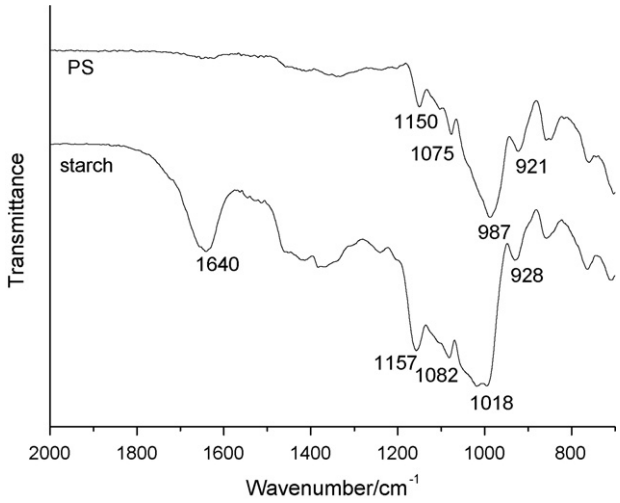

Fig. 1. The FTIR spectra of native starch and PS.

T_c are onset temperature, peak temperature and completion temperature, respectively.

3.2. Plasticization of D. opposita Thunb. starch

FTIR spectra of starch and PS are shown in Fig. 1. The characteristic peaks of starch between 990 and 1160 cm^{-1} were attributed to C–O bond stretching. The peaks at around 1157 and 1082 cm^{-1} were characteristic of C–O–H in starch, while the peak between 990 and 1020 cm^{-1} was ascribed to O–C stretch in the anhydroglucose ring. Compared to the characteristic peaks of native starch, those of PS located at the lower wave number, and the single peak appeared at 987 cm^{-1}, substituting the double-peak of native starch. The more stable and strong the hydrogen bonds were, the more the correlative peaks shifted and the peak styles changed (Ma & Yu, 2004). It should be related to the new formation of hydrogen bonds between glycerol and C–O group of starch. And the peak at 1640 cm^{-1} was related to the tightly bound water in native starch (Fang et al., 2002), which was disappear in PS. No water was bound with starch in PS. All these results indicated that starch was plasticized. The stronger hydrogen bonds were formed between glycerol and starch compared with intra- and intermolecular hydrogen bonds in native starch (Dai, Chang, Geng, Yu, & Ma, 2010).

Native starch is in the size of about 20 μm in Fig. 2(a). As shown in Fig. 2(b), no residual granular structure of starch was observed in the continuous PS phase. At the high temperature, water and glycerol were known to physically break up the granules of starch and disrupt intermolecular and intramolecular hydrogen bonds and make the native starch plastic (Ma, Jian, Chang, & Yu, 2008).

As shown in Fig. 3, the starch exhibited the typical B-type crystalline (Van Soest & Vliegenthart, 1997) with the relative crystallinity 26.9%. There were the strong diffraction peaks at 17° 2θ and a few small peaks at around 2θ values of 6°, 15°, 22° and 24°. PS had much lower degree of crystallinity than native starch. In casting process, glycerol and water molecules entered into starch granules, then could replace intermolecular and intramolecular hydrogen bonds in native starch. The crystallinity of native starch was destroyed during the casting process, so the degree of crystallinity in PS decreased.

3.3. HNT/plasticized starch composites

3.3.1. Scanning electron microscopy (SEM)

As revealed by Fig. 4(a), HNT exhibited the shape of the nanotube with the size of 10–30 nm in diameter and about 1–2 μm in length. The distribution of HNT in the matrix of PS was exhibited in Fig. 4(b)–(d). HNT could be evenly dispersed in PS matrix. A few agglomeration of HNT appeared in the HNT/PS composites with higher HNT contents. The agglomeration of HNT (9 wt% contents) was marked with white circles in Fig. 4(d). In addition, the surface of HNT appeared to be covered by PS. These could be attributed to the interaction between HNT surface and PS matrix. DNA has been found to form the supramolecular interaction with HNT surface, and increase the water solubility of HNT (Shamsi & Geckeler, 2008). Similarly, amylose can warp single-wall carbon nanotubes (Kim et al., 2003). Therefore, the interaction between HNT surface

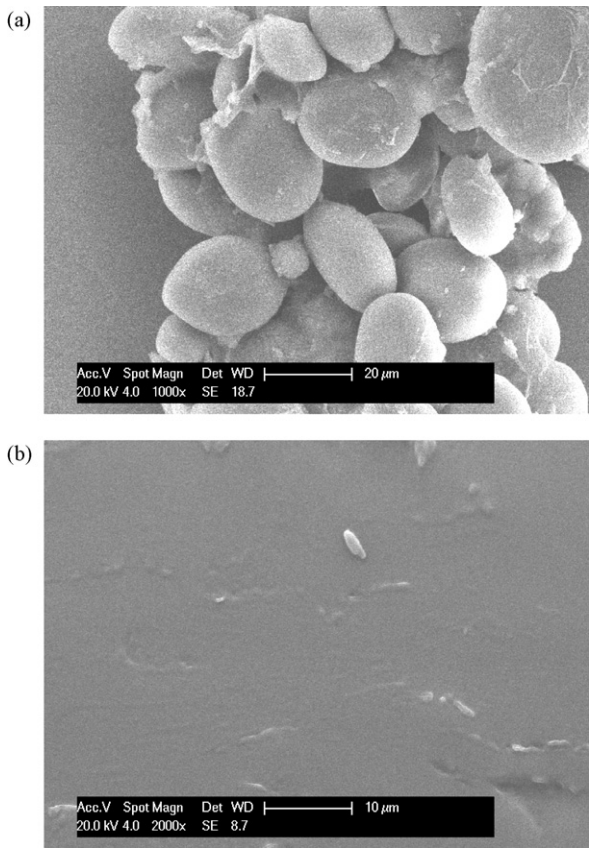

Fig. 2. SEM micrograph of native starch granules (a) and the fracture surface of PS (b).

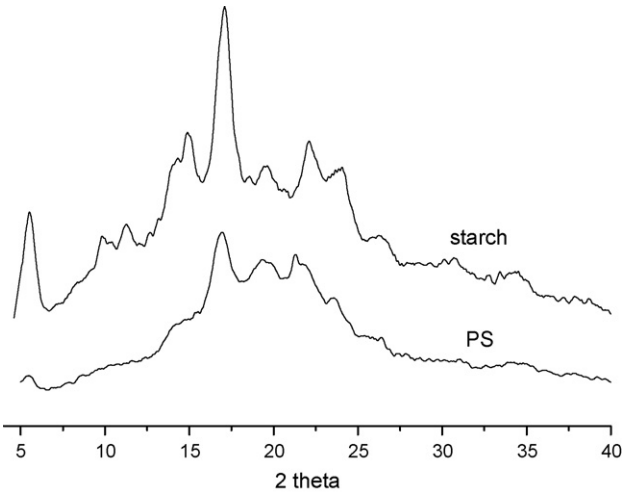

Fig. 3. The X-ray diffractograms of native starch and PS.

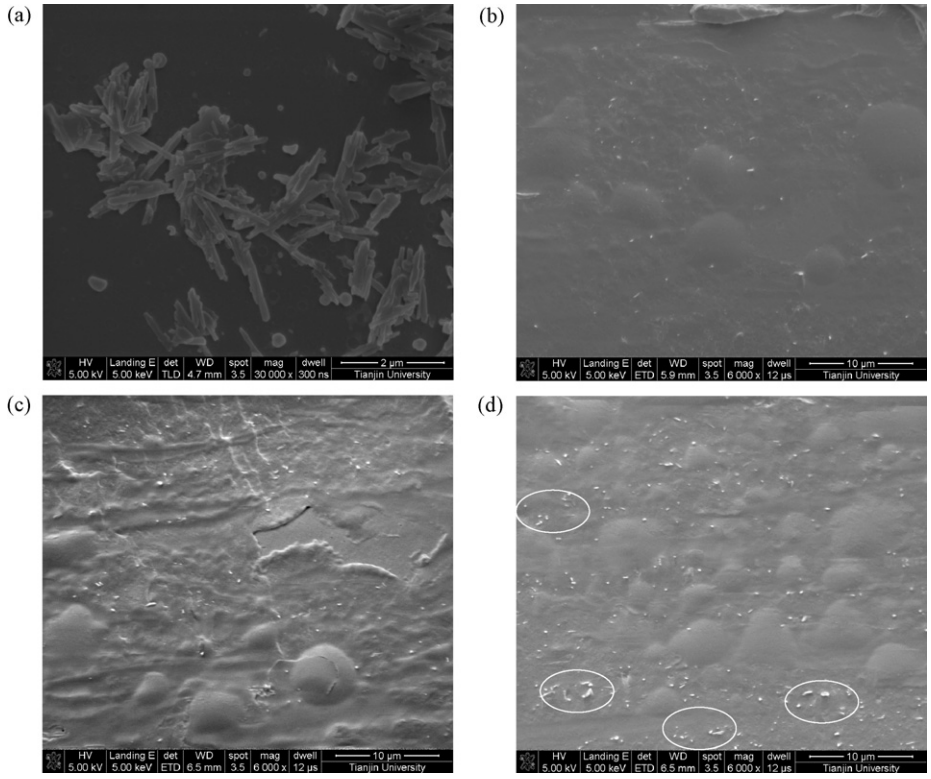

Fig. 4. SEM micrograph of HNT (a) and the fragile fractured surface for HNT/PS composites. 1.5 wt% (b), 6 wt% (c) and 9 wt% (d) HNT contents.

and starch could attribute to the similar supramolecular interaction.

3.3.2. RVA

Pasting curves for starch slurry were measured during a heating–cooling cycle to evaluate the effect of HNT contents, as shown in Fig. 5, where the temperature pattern was also shown. In order to simulate the process of preparing HNT/PS composites, the starch slurry had the same composition as the mixture used to prepare the composites. The dependence of the pasting profiles of the starch slurries on HNT contents was similar. When the granular starch began to gelatinize at elevated temperature, the viscosity of starch slurry increased. The pasting viscosity increased with the increasing of HNT contents. Since a small amount of HNT (3 wt% HNT is equivalent to about 0.15 wt% of starch slurry) resulted in profound increase in viscosity, the interaction between HNT and starch was increased presumably.

3.3.3. Mechanical testing

Fig. 6 shows the effect of HNT contents on the mechanical properties of HNT/PS composites. As the filler, HNT had an obvious enforcement effect. With increasing CN contents, the tensile strength of the composites increased, but the elongation at break decreased. When the HNT content varied from 0 to 9 wt%, the tensile strength increased from 3.9 to 9.72 MPa, while the elongation at break decreased from 12.9% to 3.7%. The increasing of tensile strength could be ascribed to the interfacial interaction between HNT and the PS matrix because of the interaction between the hydroxyl groups at the surface of HNT and PS matrix. When more

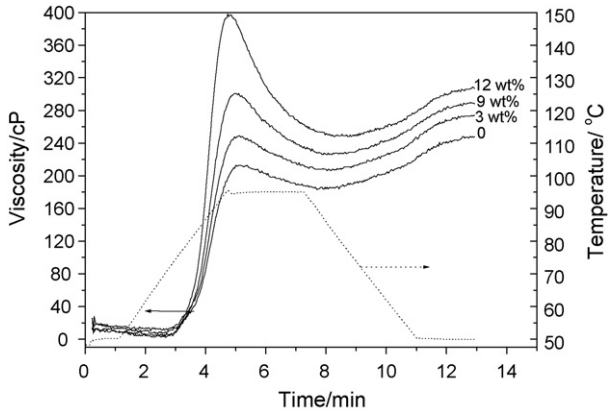

Fig. 5. The effect of HNT contents on the plots of viscometric profile. The curve (dash dot line) was the temperature profile.

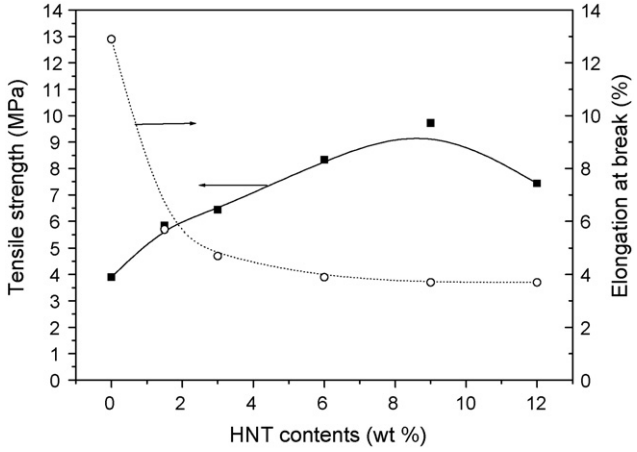

Fig. 6. The effect of HNT contents on tensile strength and elongation at break of HNT/PS composites.

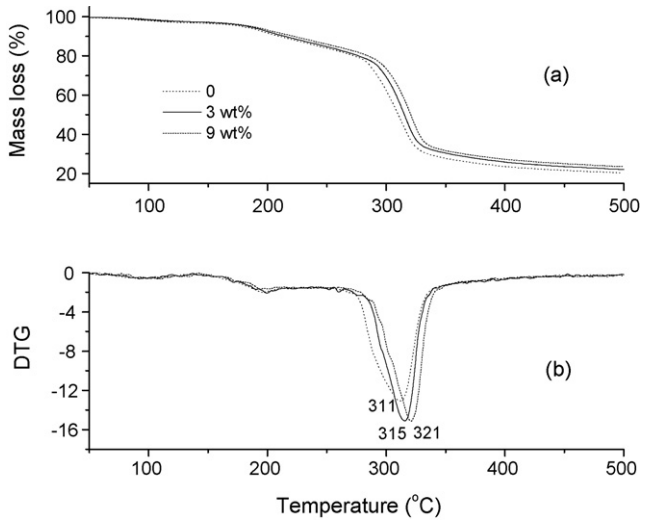

Fig. 7. The effect of HNT contents on the thermal stability of HNT/PS composites.

HNT (12 wt%) was added to the matrix, the tensile strength of the composites decreased, which may be ascribed to the agglomeration of HNT.

3.3.4. TGA

The thermogravimetric (TG) and derivative thermogravimetric (DTG) curves of PS and HNT/PS composites in nitrogen at a heating rate of 15 °C/min are shown in Fig. 7. The decomposed temperature, T_{max} was the temperature at maximum rate of mass loss, i.e. the peak temperature shown in Fig. 7(b). The degradation of PS and PS/HNT (3 and 9 wt% HNT) composites took place at 311, 315 and 321 °C, respectively. The addition of HNT increased the thermal stability of the composites. It was related to the better thermal stability of HNT and the interaction between PS and HNT.

3.3.5. Water vapor permeability (WVP)

Water vapor permeability (WVP) is used to study the moisture transport through the HNT/PS composite films. As shown in Fig. 8, WVP of HNT/PS composites decreased with the increasing of HNT contents at RH 75% and 100%. Water vapor easily went through PS film with the highest WVP values of 8.48 and 14.54×10^{-10} g m^{-1} s^{-1} Pa^{-1} at RH 75% and 100%. With the increasing of HNT contents, WVP values decreased obviously. When HNT contents reached above 6 wt%, WVP values decreased a little. Since water resistance of HNT was better than PS matrix, the addition of HNT probably introduced a tortuous path for water molecule to pass through (Chang, Jian, Zheng, Yu, & Ma, 2010). At the low HNT loading contents (below 6 wt%), HNT could disperse well in the matrix. There were few paths for water molecule to pass through. At the high contents of HNT, the aggregation of HNT could counteract the addition of HNT. Generally, the composites exhibited water vapor barrier in comparison with pure PS.

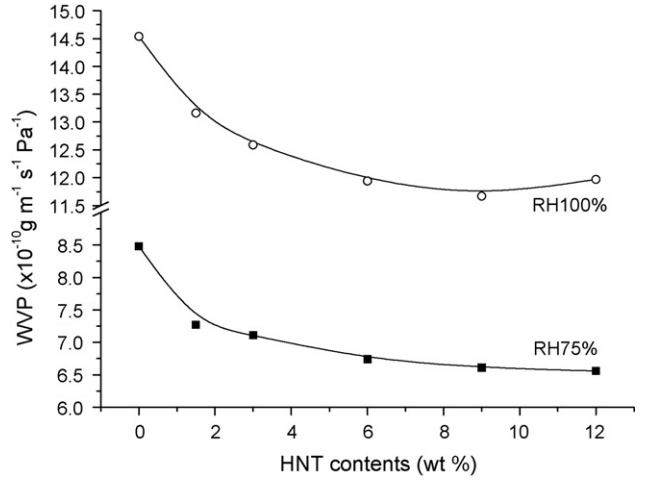

Fig. 8. The effect of HNT contents on water vapor permeability of HNT/PS composites (at RH 75% and 100%).

4. Conclusions

The starch is isolated from *D. opposita* Thunb. and characterized in terms of amylose contents, granular morphology, the degree and style of crystallinity, the transition temperatures and the enthalpy of gelatinization in this study. HNT/PS composites were prepared. The good interaction between HNT and PS imparted the improvement of the properties. HNT could obviously enhance the pasting viscosity, tensile strength and thermal stability of the composites. Also, HNT improved water vapor barrier of the composites in comparison with pure PS. This study has clearly highlighted the potential of *D. opposita* Thunb. starch to prepare plasticized materials and of HNTs to enhance the properties of plasticized starch.

Acknowledgement

This work was financially supported by the Research Fund for the Doctoral Program of Higher Education of China for Youth (Grant No. 200800561049).

References

Chang, P. R., Jian, R. J., Yu, J. G., & Ma, X. F. (2010). Fabrication and characterization of chitosan nanoparticles/plasticized-starch composites. *Food Chemistry*, *120*, 736–740.

Chang, P. R., Jian, R. J., Zheng, P. W., Yu, J. G., & Ma, X. F. (2010). Preparation and properties of glycerol plasticized-starch (GPS)/cellulose nanoparticle (CN) composites. *Carbohydrate Polymers*, *79*, 301–305.

Dai, H. G., Chang, P. R., Geng, F. Y., Yu, J. G., & Ma, X. F. (2010). Preparation and properties of starch-based film using N,N-bis(2-hydroxyethyl)formamide as a new plasticizer. *Carbohydrate Polymers*, *79*, 306–311.

Kim, O. K., Je, J., Baldwin, J. W., Kooi, S., Pehrsson, P. E., & Buckley, L. J. (2003). Solubilization of single-wall carbon nanotubes by supramolecular encapsulation of helical amylase. *Journal of the American Chemical Society*, *125*, 4426–4427.

Fang, J. M., Fowler, P. A., Tomkinson, J., & Hill, C. A. S. (2002). The preparation and characterisation of a series of chemically modified potato starches. *Carbohydrate Polymers*, *47*, 245–252.

Liu, M. X., Guo, B. C., Du, M. L., Cai, X. J., & Jia, D. (2007). Properties of halloysite nanotube-epoxy resin hybrids and the interfacial reactions in the systems. *Nanotechnology*, *18*, 455703.

Liu, M. X., Guo, B. C., Du, M. L., Zou, Q. L., & Du, M. L. (2008). Interactions between halloysite nanotubes and 2,5-bis(2-benzoxazolyl) thiophene and their effects on reinforcement of polypropylene/halloysite nanocomposites. *Nanotechnology*, *19*, 205709.

Ma, X. F., Jian, R. J., Chang, P. R., & Yu, J. G. (2008). Fabrication and characterization of citric acid-modified starch nanoparticles/plasticized-starch composites. *Biomacromolecules*, *9*, 314–3320.

Ma, X. F., & Yu, J. G. (2004). Formamide as the plasticizer for thermoplastic starch. *Journal of Applied Polymer Science*, *93*, 1769–1773.

Shamsi, M. H., & Geckeler, K. E. (2008). The first biopolymer-wrapped non-carbon nanotubes. *Nanotechnology*, *19*, 075604.

Shchukin, D. G., Sukhorukov, G. B., Price, R. R., & Lvov, Y. M. (2005). Halloysite nanotubes as biomimetic nanoreactors. *Small*, *1*, 510–513.

Wang, S. J., Liu, H. Y., Gao, W. Y., Chen, H. X., Yu, J. G., & Xiao, P. G. (2006). Characterization of new starches separated from different Chinese yam (*Dioscorea opposita* Thunb.) cultivars. *Food Chemistry*, *99*, 30–37.

Wang, S. J., Yu, J. L., Gao, W. Y., Pang, J. P., Yu, J. G., & Xiao, P. G. (2007). Comparison of starches separated from three different *F. cirrhosa*. *Journal of Food Engineering*, *80*, 417–422.

Wang, S. J., Yu, J. L., Liu, H. Y., & Chen, W. P. (2008). Characterisation and preliminary lipid-lowering evaluation of starch from Chinese yam. *Food Chemistry*, *108*, 176–181.

Wang, S. J., Yu, J. L., & Yu, J. G. (2008). The semi-crystalline growth rings of C-type pea starch granule revealed by SEM and HR-TEM during acid hydrolysis. *Carbohydrate Polymers*, *74*, 731–739.

Williams, P. C., Kuzina, F. D., & Hiynka, I. (1970). A rapid colorimetric procedure for estimation the amylose content of starches and flours. *Cereal Chemistry*, *47*, 411–420.

Van Soest, J. J. G., & Vliegenthart, J. F. G. (1997). Crystallinity in starch plastics: Consequences for material properties. *Trends in Biotechnology*, *15*, 208–213.

Yu, J. G., Wang, N., & Ma, X. F. (2008). Fabrication and characterization of poly(lactic acid)/acetyl tributyl citrate/carbon black as conductive polymer composites. *Biomacromolecules*, *9*, 1050–1057.